

Accepted to *The Astrophysical Journal* (Nov. 26, 2001)

Chandra Detection of a Type II Quasar at $z = 3.288^1$

Daniel Stern², Edward C. Moran³, Alison L. Coil³, Andrew Connolly⁴, Marc Davis^{3,5}, Steve Dawson³, Arjun Dey⁶, Peter Eisenhardt², Richard Elston⁷, James R. Graham³, Fiona Harrison⁸, David J. Helfand⁹, Brad Holden^{10,11}, Peter Mao⁸, Piero Rosati¹², Hyron Spinrad³, S.A. Stanford^{10,11}, Paolo Tozzi^{13,14}, & K.L. Wu⁷

ABSTRACT

¹Some of the data presented herein were obtained at the W.M. Keck Observatory, which is operated as a scientific partnership among the California Institute of Technology, the University of California and the National Aeronautics and Space Administration. The Observatory was made possible by the generous financial support of the W.M. Keck Foundation. Based on observations with the NASA/ESA *Hubble Space Telescope*, obtained at the Space Telescope Science Institute, which is operated by the Association of Universities for Research in Astronomy, Inc. under NASA contract No. NAS5-26555. Based on observations at the Kitt Peak National Observatory, National Optical Astronomy Observatory, which is operated by the Association of Universities for Research in Astronomy, Inc. under cooperative agreement with the National Science Foundation.

²Jet Propulsion Laboratory, California Institute of Technology, Mail Stop 169-327, Pasadena, CA 91109 USA [email: stern@zwolfkinder.jpl.nasa.gov]

³Department of Astronomy, University of California at Berkeley, Berkeley, CA 94720 USA

⁴Department of Physics and Astronomy, University of Pittsburgh, Pittsburgh, PA 15260 USA

⁵Department of Physics, University of California at Berkeley, Berkeley, CA 94720 USA

⁶Kitt Peak National Observatory, 950 North Cherry Avenue, Tucson, AZ 85719 USA

⁷Department of Astronomy, The University of Florida, P.O. Box 112055, Gainesville, FL 32611 USA

⁸Division of Physics, Mathematics and Astronomy, 105–24, California Institute of Technology, Pasadena, CA 91125 USA

⁹Columbia University, Department of Astronomy, 550 West 120th Street, New York, NY 10027 USA

¹⁰Institute of Geophysics and Planetary Physics, Lawrence Livermore National Laboratory, L-413, Livermore, CA 94550 USA

¹¹Physics Department, University of California at Davis, Davis, CA 95616 USA

¹²European Southern Observatory, Karl-Schwarzschildstr. 2, D-85748, Garching, Germany

¹³Department of Physics and Astronomy, The Johns Hopkins University, Baltimore, MD 21218 USA

¹⁴Osservatorio Astronomico di Trieste, via G.B. Tiepolo 11, I-34131, Trieste, Italy

We report on observations of a Type II quasar at redshift $z = 3.288$, identified as a hard X-ray source in a 185 ks observation with the *Chandra X-ray Observatory* and as a high-redshift photometric candidate from deep, multiband optical imaging. CXO J084837.9+445352 (hereinafter CXO52) shows an unusually hard X-ray spectrum from which we infer an absorbing column density $N_{\text{H}} = (4.8 \pm 2.1) \times 10^{23} \text{ cm}^{-2}$ (90% confidence) and an implied unabsorbed 2–10 keV rest-frame luminosity of $L_{2-10} = 3.3 \times 10^{44} \text{ ergs s}^{-1}$, well within the quasar regime. *Hubble Space Telescope* imaging shows CXO52 to be elongated with slight morphological differences between the WFPC2 F814W and NICMOS F160W bands. Optical and near-infrared spectroscopy of CXO52 show high-ionization emission lines with velocity widths $\sim 1000 \text{ km s}^{-1}$ and flux ratios similar to a Seyfert 2 galaxy or radio galaxy. The latter are the only class of high-redshift Type II luminous AGN which have been extensively studied to date. Unlike radio galaxies, however, CXO52 is radio quiet, remaining undetected at radio wavelengths to fairly deep limits, $f_{4.8\text{GHz}} < 40\mu\text{Jy}$. High-redshift Type II quasars, expected from unification models of active galaxies and long-thought necessary to explain the X-ray background, are poorly constrained observationally with few such systems known. We discuss recent observations of similar Type II quasars and detail search techniques for such systems: namely (1) X-ray selection, (2) radio selection, (3) multi-color imaging selection, and (4) narrow-band imaging selection. Such studies are likely to begin identifying luminous, high-redshift Type II systems in large numbers. We discuss the prospects for these studies and their implications to our understanding of the X-ray background.

Subject headings: cosmology: observations – X-rays: galaxies – galaxies: active – galaxies: individual (CXO J084837.9+445352)

1. Introduction

Unified models of active galactic nuclei (AGN) posit orientation and intrinsic luminosity as the two primary physical parameters governing the optical characteristics of an active galaxy (e.g., Antonucci 1993; Urry & Padovani 1995). According to these models, when the obscuring torus of an AGN is oriented perpendicular to the observer line of sight, one sees spatially-unresolved, Doppler-boosted emission from hot gas near the central supermassive black hole in the form of broad ($\text{FWHM} = 5000 - 20000 \text{ km s}^{-1}$), high-ionization emission lines and synchrotron emission from the central nucleus in the form of power-law ultraviolet/optical continuum emission. Independent of orientation one sees narrow emission lines

(FWHM = 500–1500 km s^{−1}) from the spatially-extended narrow-line region. When the line of sight to the central engine is blocked by the torus, only the extended narrow-line emission is seen. Active galaxies without observed broad emission lines but with high-ionization species are classified as Type II systems, while those with broad line emission are classified Type I. In addition to the narrow line region, hard X-ray, far-infrared, and radio emission from AGN are also largely immune to obscuration and orientation effects.

Intrinsic, unobscured luminosity, or activity level, is the second primary physical parameter differentiating AGN. The most luminous active galaxies ($−30 \lesssim M_B \lesssim −23$), where light from the central regions overwhelm evidence of the underlying stellar populations, are identified as quasars (QSOs). At lower luminosity ($M_B \gtrsim −23$), Seyfert galaxies show evidence of both host galaxy stellar emission and radiation from the central AGN. Finally, surveys of local galaxies find a class of sources with very low power, low-ionization nuclear emitting regions, LINERs, which are likely the lethargic cousins of the luminous active galaxies. About one third of all galaxies show evidence of low-power AGNs, seen in the form of either LINERs or low-luminosity Seyferts (e.g., Ho 1999). This briefly-described unification model is supported by a variety of observations, including reverberation mapping, polarization studies, and mapping of the ionized gas morphology.

Surveys of bright galaxies have characterized the local demographics of AGN: the fraction of field galaxies which are classified as Seyferts rises from approximately 1% at $M_{pg} = −21$ to essentially all galaxies at $M_{pg} = −23$ (Meurs 1982; Meurs & Wilson 1984). The local ratio of obscured (Type II) to unobscured (Type I) Seyferts is approximately 4:1 (Osterbrock & Shaw 1988). At high redshift, the Type I quasars are well-characterized, with the luminosity function measured out to $z \sim 5$ and individual examples known out to redshift $z = 6.28$ (Fan et al. 2001). Our knowledge of Type II quasars, however, is observationally sparse with many fewer examples known (e.g., Urry & Padovani 1995). Because of the obscuration, Type II quasars are not identified at high redshift from shallow large-area sky surveys, though low-redshift examples are beginning to be uncovered due to their unusual colors caused by high-equivalent width emission features (e.g., Djorgovski et al. 2001a). Hard (2–10 kev) X-ray surveys have identified several examples (e.g., Norman et al. 2001). Importantly, but surprisingly neglected in much of the X-ray Type II quasar literature, radio surveys have been detecting the radio-loud end of the Type II quasar population for several decades: these sources are called radio galaxies (see McCarthy 1993, for a comprehensive review) and they have been identified out to redshift $z = 5.19$ (van Breugel et al. 1999).

The abundance of Type II QSOs at high redshift is of considerable interest for models of the X-ray background (XRB). Stellar sources, hot gas associated with galaxies, and Type I AGN appear to be insufficient to explain the XRB. Most models invoke a substantial

population of luminous, Type II AGN to produce the 2–10 keV background, with values of the ratio of obscured to unobscured luminous AGN at $z \sim 1$ ranging from 4:1 to 10:1 (e.g., Madau, Ghisellini, & Fabian 1994; Comastri et al. 1995). However, few examples of this population have been observed. If these sources are indeed shown to exist in such multitudes, they must indeed make an important contribution to the XRB.

The abundance of Type II QSOs at high redshift may also prove interesting in terms of understanding which sources are responsible for ionizing the early Universe (Becker et al. 2001; Djorgovski et al. 2001b). Does the ultraviolet light produced by hot stars in young protogalaxies ionize the intergalactic medium at $z \gtrsim 6$? Or does ultraviolet light from obscured and unobscured AGN cause this phase change in the early Universe?

Several examples of Type II quasars at low to intermediate redshift have been suggested from X-ray surveys prior to *Chandra* — e.g., *IRAS* 20181–2244 at $z = 0.185$ (rest-frame 2–10 kev luminosity $L_{2-10} = 2.2 \times 10^{44} \text{ ergs s}^{-1}$; Elizalde & Steiner 1994), 1E 0449.4–1823 at $z = 0.338$ ($L_{2-10} = 6.7 \times 10^{44} \text{ ergs s}^{-1}$; Stocke et al. 1982), AXJ0341.4–4453 at $z = 0.672$ ($L_{2-10} = 1.8 \times 10^{44} \text{ ergs s}^{-1}$; Boyle et al. 1988), and RX J13434+0001 at $z = 2.35$ ($L_{2-10} \sim 5 \times 10^{45} \text{ ergs s}^{-1}$; Almaini et al. 1995, Georgantopoulos et al. 1999). In all four cases, subsequent spectroscopy revealed broad Balmer emission lines, leading Halpern and collaborators (Halpern & Moran 1998; Halpern, Eracleous, & Forster 1998; Halpern, Turner, & George 1999) to reclassify such Type II quasar candidates as narrow-lined Seyfert 1 (NLS1) galaxies — i.e., *not* as high-luminosity analogs of Seyfert 2 galaxies. According to the definitions of Osterbrock & Pogge (1985) and Goodrich (1989), NLS1s have FWHM $H\beta < 2000 \text{ km s}^{-1}$, $[\text{O III}] \lambda 5007 / H\beta < 3$, and often show emission lines from Fe II or higher-ionization iron lines such as $[\text{Fe VII}] \lambda 6087$ and $[\text{Fe X}] \lambda 6375$. In contrast, Seyfert 2 galaxies generally have $[\text{O III}] \lambda 5007 / H\beta > 3$ and no permitted Fe II emission. In terms of studying the XRB the distinction may be pedantic: both systems refer to high-luminosity obscured AGN whose space density at high redshift are poorly known and thus may be important contributors to the hard (2–10 keV) XRB. However, in terms of studying the physics of active galaxies, the distinction is far from pedantic. NLS1 galaxies have visual absorptions of a few to a few tens of magnitudes while Compton-thick Seyfert 2 galaxies show visual absorptions of 1000 magnitudes or more, inferred from their X-ray-determined column densities (see Halpern et al. 1999). With distinctly steeper optical and X-ray spectra and more rapid X-ray variability relative to normal Seyfert 1s and Seyfert 2s, NLS1s elude explanation within the orientation-dependent unification scheme of Seyfert galaxies. Finally, unlike Seyfert 2 galaxies, NLS1s are not limited to low luminosity: several of the PG quasars (Boroson & Green 1992) are classified as NLS1s according to the definitions above. The lack of high-luminosity analogs of Seyfert 2s might imply that all sufficiently luminous QSO nuclei are able to clear Compton-thick absorbing material from their vicinity, affording detection

of the broad-line region from all viewing angles.

We describe observations of one luminous, high-redshift ($z = 3.288$), Type II quasar candidate, CXO J084837.9+445352, hereinafter CXO52, identified as the 52nd object in our 185 ks *Chandra* observation of the Lynx field (see Stern et al. 2001b). The Lynx field is one of four fields which comprise the Spectroscopic Photometric Infrared-Chosen Extragalactic Survey (SPICES; Eisenhardt et al. 2001; Stern et al. 2001a). CXO52 was identified independently both as an optical, color-selected, high-redshift source (e.g., Stern et al. 2000c) and from optical follow-up of X-ray sources in the Lynx field. The Lynx field contains three known X-ray emitting clusters out to redshift $z = 1.27$ (Stanford et al. 1997; Rosati et al. 1998, 1999). Analyses of the *Chandra* data for these clusters are described in Stanford et al. (2001) and Holden et al. (2001). We note that gravitational lensing due to the $\approx 30''$ distant $z = 1.27$ galaxy cluster RX J0848+4453 has not significantly brightened CXO52. For the cluster velocity dispersion $\sigma = 650 \text{ km s}^{-1}$ (Stanford et al. 2001), CXO52 is magnified by less than 10%. In §2 we describe the multiwavelength observations of CXO52 which span the X-ray to radio. In §3 we discuss CXO52 in terms of both AGN unification schemes and the implications for the XRB. Section 4 summarizes our results.

We assume $H_0 = 50 h_{50} \text{ km s}^{-1} \text{ Mpc}^{-1}$, $\Omega_M = 1$, and $\Omega_\Lambda = 0$ throughout. For this cosmology, the luminosity distance of CXO52 is $26.61 h_{50}^{-1} \text{ Gpc}$ and one arcsecond subtends $7.02 h_{50}^{-1} \text{ kpc}$. For $H_0 = 65 \text{ km s}^{-1} \text{ Mpc}^{-1}$, $\Omega_M = 0.35$, and $\Omega_\Lambda = 0.65$, the cosmology favored by recent high-redshift supernovae and cosmic microwave background observations (e.g., Riess et al. 2001), these distances change only slightly: both are larger by 9.6%.

2. Observations and Results

2.1. Ground-Based Optical/Near-Infrared Imaging

CXO52 was initially identified from deep *BRIz* imaging using the “dropout” color selection techniques which have proved successful at identifying high-redshift galaxies (e.g., Steidel et al. 1996; Dey et al. 1998; Spinrad et al. 1998; Stern & Spinrad 1999) and quasars (e.g., Kennefick, Djorgovski, & de Calvalho 1995; Fan et al. 1999; Stern et al. 2000c). The selection criteria rely upon absorption from the Lyman break and Lyman forests attenuating the rest-frame ultraviolet continua of high-redshift sources. Long-ward of Ly α , both star-forming galaxies and quasars have relatively flat (in f_ν) continua. Together, these features provide such systems with a largely unambiguous locus in multidimensional color-color space. In concept, the multicolor survey pursued by a subset of the authors is similar to established quasar surveys relying upon the digitized Palomar Sky Survey (e.g., Djorgovski et al. 1999)

and the Sloan Digital Sky Survey (e.g., Fan et al. 1999). In practice, we probe a much smaller area of sky (eventually a few 100 arcmin² rather than $\pi - 2\pi$ steradians) to much fainter magnitudes (eventually $\approx 27^{\text{th}}$ mag AB rather than $\approx 21^{\text{st}}$ mag AB). Our survey has identified numerous sources at $z > 3$, including the faint quasar RD J030117+002025 at $z = 5.50$ which was the most distant quasar at the time of its discovery and remains the lowest luminosity quasar known at $z > 4$ (Stern et al. 2000c).

We obtained optical $BRIz$ imaging using the Kitt Peak National Observatory (KPNO) 4 m Mayall telescope with its Prime Focus CCD imager (PFCCD) equipped with a thinned 2048 \times 2048 array. This configuration gives a 16' \times 16' field of view with 0''.47 pix⁻¹. We used a Harris B -band ($\lambda_c = 4313$ Å; $\Delta\lambda = 1069$ Å), Harris R -band ($\lambda_c = 6458$ Å; $\Delta\lambda = 1472$ Å), Harris I -band ($\lambda_c = 8204$ Å; $\Delta\lambda = 1821$ Å), and an RG850 long-pass z -band filter. The combined, processed images reach limiting AB magnitudes of 26.8 (B), 25.6 (R), 25.1 (I), and 24.7 (z), where these numbers represent 3 σ limits in 3'' diameter apertures. The corresponding Vega magnitude limits are 26.9, 25.4, 24.6, and 24.2, respectively.

We obtained near-infrared JK_s imaging at the KPNO 4 m with the Infrared Imager (IRIM; Fowler et al. 1988) equipped with a NICMOS 3 256 \times 256 HeCdTe array giving 0''.6 pix⁻¹. The J -band ($\lambda_c = 1.14\mu\text{m}$; $\Delta\lambda = 0.29\mu\text{m}$) imaging reaches a 3 σ limiting magnitude of 22.9 (Vega) in a 3'' diameter aperture. The K_s -band ($\lambda_c = 2.16\mu\text{m}$; $\Delta\lambda = 0.33\mu\text{m}$) imaging reaches a corresponding depth of $K_s = 21.4$. These $BRIzJK_s$ Kitt Peak images comprise one field in the SPICES field galaxy survey. Data reduction for the optical and near-infrared imaging followed standard techniques (for details, see Eisenhardt et al. 2001).

We supplemented the KPNO optical imaging with deep imaging at Palomar Observatory. On UT 1999 November 11–12, we used the COSMIC camera (Kells et al. 1998) on the 200'' Hale telescope to obtain extremely deep (5.1 hr) Kron-Cousins R -band ($\lambda_c = 6200$ Å; $\Delta\lambda = 800$ Å) imaging of the Lynx field and on UT 2000 April 30 – May 1 we used the same camera/telescope configuration to obtain a 3.2 hr image through a Gunn i filter ($\lambda_c = 8000$ Å; $\Delta\lambda = 1800$ Å). COSMIC uses a 2048 \times 2048 pixel thinned CCD with 0''.2846 pix⁻¹, providing a 9''.7 \times 9''.7 field of view. These images, obtained with the purpose of identifying high-redshift candidates, reach limiting magnitudes of 26.5 and 25.5 mag respectively (Vega; 3 σ in 3'' diameter apertures). Several B - and R -band dropouts were identified from the optical data, many of which have subsequently been confirmed to reside out to redshifts of $z = 5.63$ and will be discussed in a future manuscript. Photometry for CXO52 is given in Table 1. This source has a relatively flat (in f_ν) spectrum from R to z , but shows a dramatic drop shortward of R with $B - R = 2.2$: CXO52 is an ideal B -band dropout candidate, exhibiting optical colors corresponding to a photometric redshift $z \approx 3.5$. With $I - K = 4.2$, CXO52 also fits within the conventional definition of an extremely red object

Fig. 1.— Images of CXO52 obtained with WFPC2/F814W (**left**) and NICMOS/F160W (**right**) on *HST*. The field of view shown is 60" on a side. North is up, and east is to the left. CXO52, located at $\alpha = 08^h48^m37.9^s$, $\delta = +44^\circ53'51''.8$ (J2000), is centered in the images, and is offset from bright star S (F814W image) by $\Delta\alpha = -11''.4$, $\Delta\delta = -26''.8$. Contours show *Chandra* X-ray imaging of this field. The inset, 2" on side, shows the resolved morphology of CXO52.

(ERO; $I - K > 4$), an intriguing population likely due to a mixture of old stellar populations at $z \sim 1.5$ and dusty systems at $z > 1$ (e.g., Dey et al. 1999).

2.2. *HST* Optical/Near-Infrared Imaging

CXO52 is only 30" ENE of the $z = 1.27$ X-ray emitting cluster RX J0848+4453 (Stanford et al. 1997, 2001; van Dokkum et al. 2001) and therefore lies within *Hubble Space Telescope* (*HST*) images of that system obtained with both the Wide Field Planetary Camera 2 (WFPC2; Trauger et al. 1994) and the Near-Infrared Camera and Multi-Object Spectrograph (NICMOS; Thompson et al. 1999). The WFPC2 images were taken on UT 1999 March 1 in the F814W (I_{814}) filter and comprise a total of 27.8 ks of integration. A mosaic of three NIC3 pointings in the F160W ($H_{1.6}$) filter were taken on UT 1998 June 5–6 during the campaign when the *HST* secondary was moved to optimized focus for Camera 3. Each pointing received approximately 11.2 ks of integration. The *HST* imaging and reductions are discussed in greater detail by van Dokkum et al. (2001).

The *HST* images of CXO52 are shown in Fig. 1. The galaxy is extended by roughly 1"0 at a position angle of approximately -25° . In 3" diameter apertures, CXO52 has AB magnitudes of 24.8 ± 0.2 through the F814W filter and 23.8 ± 0.3 through the F160W filter. Morphologically, CXO52 appears to be an interacting system, with an extended southern component, dominating the measured position angle, and a compact northern component. Comparison of the insets in Fig. 1 shows a slight chromatic variation in the morphology of CXO52. Relative to the F160W image, the centroid of the northern component appears $\approx 0''.1$ farther to the east in the F814W image.

2.3. *Chandra* X-ray Data

The Advanced CCD Imaging Spectrometer (ACIS-I) on board the *Chandra X-ray Observatory* (Weisskopf, O’dell, & van Speybroeck 1996) obtained a 184.7 ks image of the Lynx field on UT 2000 May 3–4. Stern et al. (2001b) discuss reduction of the X-ray data and the identification of optical and near-infrared counterparts to the 153 compact X-ray sources in the field. A total of ~ 54 net counts were detected at the position of the *B*-band dropout galaxy described above. The source hardness ratio based on the counts detected in soft (0.5–2.0 keV; S) and hard (2.0–7.0 keV; H) energy bands is $(H - S)/(H + S) = 0.07 \pm 0.13$. We detect no variability in the X-ray flux or spectrum. Assuming the flux spectrum can be expressed as a simple power-law function of energy E (i.e., $F(E) \propto E^\alpha$) modified by the Galactic absorption column density in the direction of the source ($N_{\text{H}} = 2 \times 10^{20} \text{ cm}^{-2}$), this hardness ratio corresponds to a spectral index of $\alpha \approx +0.5$ (Stern et al. 2001b) — quite unlike the steep $\alpha \approx -0.8$ spectra that are commonly observed for unabsorbed AGNs (e.g., Nandra & Pounds 1994). Given the narrow-line optical/UV spectrum of the source (see §2.5 below), it is likely that CXO52 actually has an intrinsically steep X-ray spectrum that appears to be flat due to significant soft X-ray absorption by intervening material within the galaxy.

To investigate this possibility, we have examined the X-ray spectrum of CXO52 more closely. Using version 2.1.2 of the *Chandra* Interactive Analysis of Observations (CIAO) software, we extracted source counts within a $6''$ radius aperture centered on the source; background was measured within a concentric annulus with inner and outer radii of $10''$ and $20''$, respectively. A response matrix and an effective area file were generated for the location of the source on chip 0, which is $\sim 3'$ from the ACIS-I aimpoint. The 0.5–8 keV spectrum was binned into five channels containing a minimum of 11 counts each for modeling with XSPEC, the X-ray spectral fitting package (Arnaud 1996). Assuming a Galactic $N_{\text{H}} = 2 \times 10^{20} \text{ cm}^{-2}$, a power-law fit to the spectrum yields a spectral index of $\alpha = +0.5$, consistent with the measured hardness ratio. If we allow for the possibility of additional absorption at the redshift of the source and fix the spectral index at a “typical” AGN value of $\alpha = -0.8$, we obtain a best-fit column density of $(4.8 \pm 2.1) \times 10^{23} \text{ cm}^{-2}$ (90% confidence) local to CXO52, similar to the column densities observed in nearby Seyfert 2 galaxies (e.g., Bassani et al. 1999). In addition, our model implies an unabsorbed 2–10 keV rest-frame luminosity of $3.3 \times 10^{44} \text{ ergs s}^{-1}$, which is well within the quasar regime. Thus, the *Chandra* data, despite their limited statistics, provide compelling evidence that CXO52 is indeed an obscured, luminous AGN.

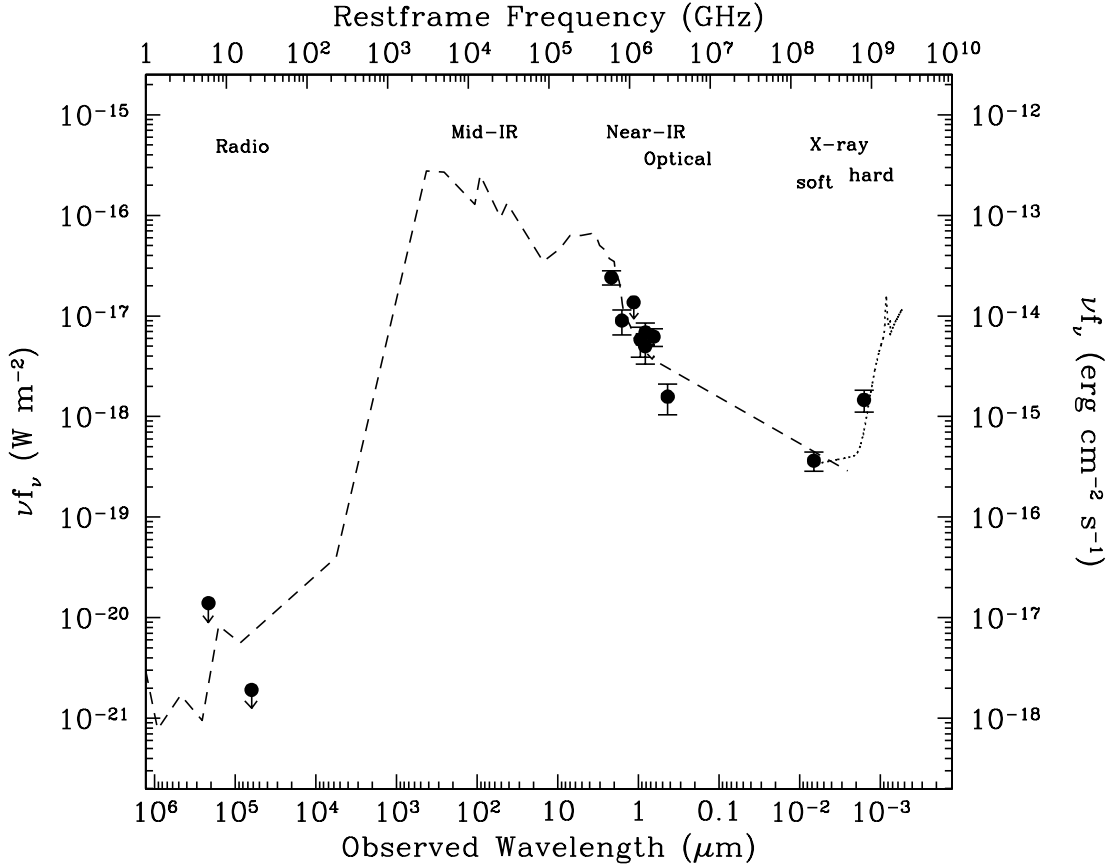


Fig. 2.— Photometry for CXO52 plotted with the scaled average spectral energy distribution (SED) for a Seyfert 2 galaxy. The dashed line shows the broad-band (radio to soft X-ray) SED composed from a sample of 15 local Seyfert 2 galaxies (Schmitt et al. 1997). The dotted line shows the composite 1–10 keV X-ray spectrum derived by Moran et al. (2001) from a distance-limited sample of 29 Seyfert 2s observed with the *Advanced Satellite for Cosmology and Astrophysics (ASCA)*.

2.4. Radio Imaging

CXO52 remains undetected in our deep, 4.8 GHz radio map of the Lynx field, obtained at the Very Large Array (VLA) on UT 1999 May 29. The VLA was in configuration D for these data and the total integration time spent on source is 11.9 ks. In source-free regions adjacent to the quasar, the root-mean-squared (rms) noise of the radio image is 14 μ Jy. However, deriving an upper limit from the object's location is complicated by the presence of a 0.29 mJy source $\approx 15''$ to the west; summing the flux density within a ≈ 330 arcsec 2 synthesized beam area centered on the quasar position yields a value of 41 μ Jy, dominated by the wings of the adjacent object. We adopt an upper limit of $f_{4.8\text{GHz}} = 40$ μ Jy. Comparison

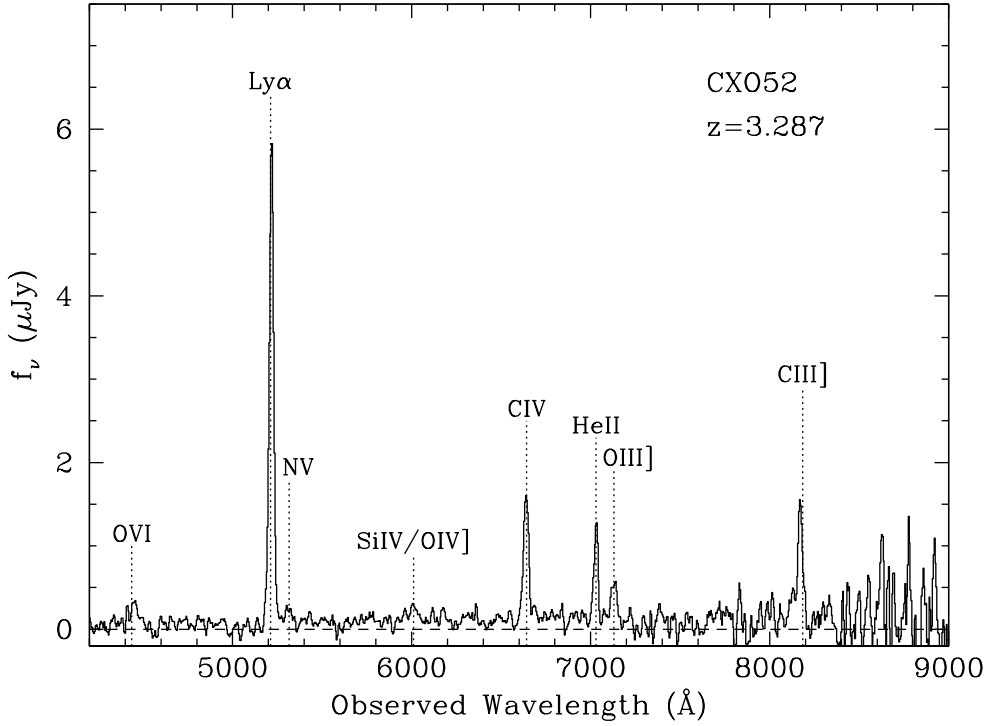


Fig. 3.— Optical spectrum of CXO52 obtained with the Keck I telescope. The optical spectrum was extracted using a $1''.5 \times 1''.5$ aperture and smoothed with a 15\AA boxcar filter. Prominent emission features are labeled.

with the 1.4 GHz FIRST (Faint Images of the Radio Sky at Twenty-Centimeters) survey (Becker, White, & Helfand 1995) reveals no radio source within $30''$ of the quasar to a limiting flux density of $f_{1.4\text{GHz}} \simeq 1 \text{ mJy}$ (5σ).

Fig. 2 illustrates the broad-band spectral energy distribution (SED) of CXO52 from our imaging observations which span nearly 10 orders of magnitude in wavelength. CXO52 well matches the average local Seyfert 2 SED derived by Schmitt et al. (1997) and Moran et al. (2001). The observed B -band flux is significantly diminished relative to the composite, naturally explained by absorption due the Ly α forest for a source at $z = 3.288$. The hard X-ray spectrum of CXO52 and the composite Seyfert 2 are indicative of obscured, luminous central engines. The non-detection of CXO52 in our radio data suggests that this galaxy is approximately a factor of three less radio-luminous than the average Seyfert 2. Ho & Ulvestad (2001), however, show that Seyfert nuclei exhibit a wide range in radio properties and powers. We conclude that the photometry of CXO52 matches the spectral shape (SED) of a high-redshift, luminous Seyfert 2, albeit with a higher bolometric luminosity.

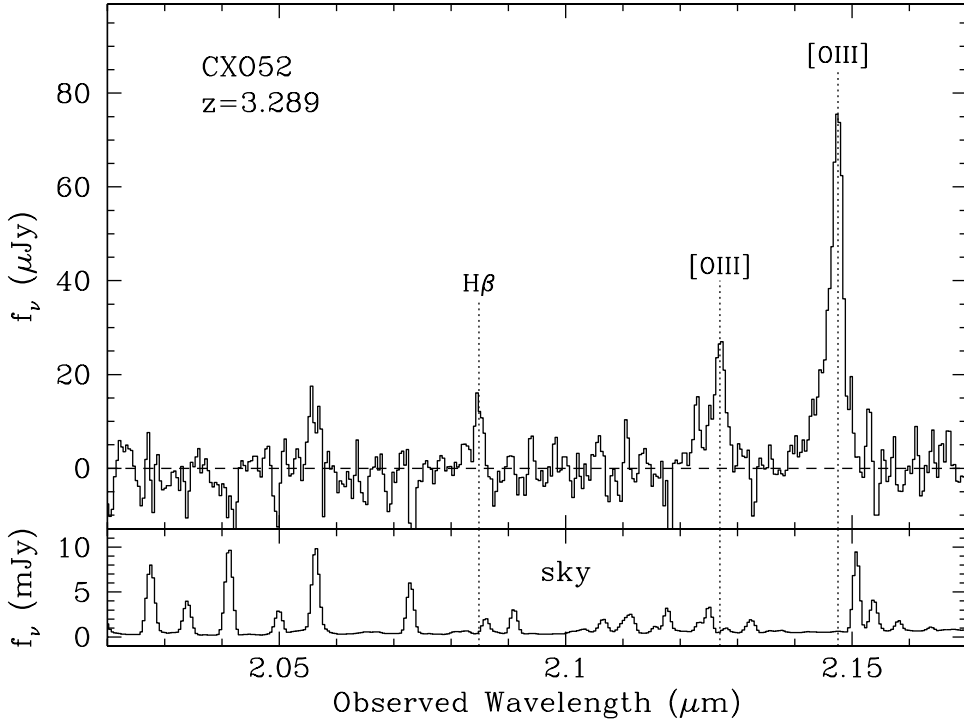


Fig. 4.— Near-infrared spectra of CXO52 and the night sky, obtained with the Keck II telescope. The spectra were extracted using $0''.57 \times 1''.35$ apertures. Prominent emission features are labeled. Note that the absorption feature at $2.042 \mu\text{m}$ and the emission feature at $2.056 \mu\text{m}$ are both artifacts due to poor subtraction of telluric OH emission.

2.5. Optical/Near-Infrared Spectroscopy

We obtained an optical spectrum of CXO52 on UT 2000 January 11 with the Low Resolution Imaging Spectrometer (LRIS; Oke et al. 1995) on the Keck I telescope. These observations, taken prior to the X-ray imaging, were in multiobject mode using a slitmask designed to study high-redshift Lyman-dropout candidates. The observations, taken at a position angle of -108.4° through a $1''.5$ slitlet, used the $150 \text{ lines mm}^{-1}$ grating ($\lambda_{\text{blaze}} = 7500 \text{\AA}$; resolution $R \approx 440$) and coarsely sample the wavelength range 4000\AA to $1 \mu\text{m}$. Three equal integrations comprise the 1.5 hr exposure and we performed $3''$ spatial offsets between integrations in order to facilitate removal of fringing at long wavelengths. As these observations did not use an order-blocking filter, 2^{nd} -order light might contribute at long wavelengths. In practice, for a faint, red source such as CXO52, this contamination is negligible. We calculated the dispersion using a NeAr lamp spectrum obtained through the mask immediately subsequent to the science observations and adjusted the wavelength zeropoint using telluric emission lines. The night was photometric with $0''.6$ seeing and the

spectrum was flux-calibrated using observations of standard stars from Massey & Gronwall (1990). The optical spectrum is shown in Fig. 3.

On UT 2001 February 3 we observed CXO52 with the Near Infrared Echelle Spectrograph (NIRSPEC; McLean et al. 1998) at the Nasmyth focus of the Keck II telescope. These observations were taken at a position angle of -24.22° through the $0''.57$ wide slit in the low dispersion mode (75 lines mm^{-1} grating), providing $0''.193 \text{ pix}^{-1}$ and a resolution $R \approx 1655$. Our spectrum represents 50 minutes of integration split into 10 minute dithered exposures, and samples the wavelength range $1.91 - 2.32 \mu\text{m}$. Wavelength calibration was performed using a NeAr lamp spectrum obtained through the slit immediately subsequent to the science observations. Comparison to telluric OH emission in those observations show the wavelength solution to be good to better than 1 \AA . The spectrum was flux-calibrated using observations of the B8 V star HD40724 observed at a similar airmass earlier in the night. The near-infrared spectrum is shown in Fig. 4.

The spectra of CXO52 are dominated by several narrow ($\text{FWHM} \gtrsim 1000 \text{ km s}^{-1}$), high-equivalent-width ($W_{\lambda, \text{obs}} \gtrsim 500 \text{ \AA}$) emission features. The unambiguous line identifications and parameters, calculated for single Gaussian fits using the **SPECFIT** contributed package within IRAF (Kriss 1994), are presented in Table 2. The measured redshift is 3.288 ± 0.001 .

3. Discussion

3.1. Morphology

CXO52 is clearly resolved and elongated in the *HST* images (Fig. 1). At a redshift of 3.288, the emission extends over $\approx 7 h_{50}^{-1} \text{ kpc}$. The WFPC2 F814W filter samples the rest-frame wavelength range $\lambda\lambda 1700 - 2200 \text{ \AA}$ for CXO52, which includes the C III] $\lambda 1909$ emission line. The observed equivalent width of this feature (Table 2) implies that the observed F814W morphology is strongly dominated by line emission. The NICMOS F160W filter samples rest-frame $\lambda\lambda 3300 - 4200 \text{ \AA}$ at this redshift, which includes the [O II] $\lambda\lambda 3726, 3729$ emission doublet. No *H*-band spectrum of CXO52 has been obtained as yet, but based on the current spectroscopy and typical radio galaxy spectra, the observed F160W morphology is again likely to be strongly dominated by line emission. Similarly, based on the NIRSPEC spectroscopic results, the *K*-band photometry is dominated by the [O III] $\lambda 5007$ emission doublet. Extended emission-line nebulae are commonly seen in powerful radio galaxies with spatial scales up to $\approx 400 \text{ kpc}$ (e.g., McCarthy, Spinrad, & van Breugel 1995).

The morphologies measured in the *HST* images reflect the distribution of UV light in CXO52, corresponding to a wavelength where extinction due to dust is most effective. The

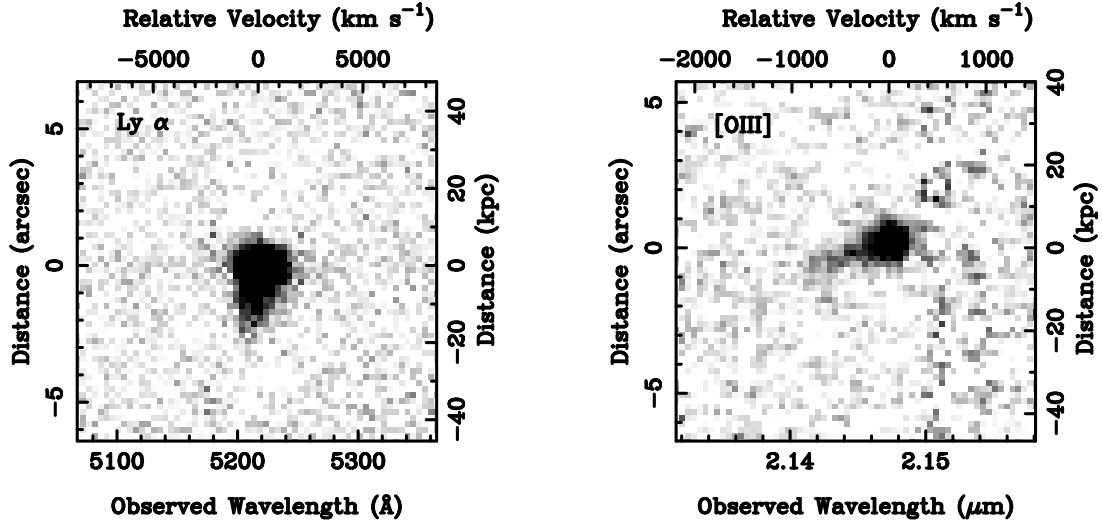


Fig. 5.— Spatially-resolved spectroscopy for the Ly α and [O III] λ 5007 emission lines of CXO52, obtained with the Keck telescopes. The LRIS observation of Ly α (left) is through a $1''.5$ slit at a position angle of -108.4° . The NIRSPEC observation of [O III] λ 5007 (right) is through a $0''.57$ slit at a position angle of -24.2° . Velocities are relative to line center. Distances are relative to peak of line brightness, with right axes in units of h_{50}^{-1} kpc. Note the sky-line residual at $2.151\ \mu\text{m}$ in the infrared spectrum.

peculiar morphology may be due to a merger system or tidal interactions, or may simply reflect the distribution of dust in the galaxy. In particular, the morphological difference in the location of the northern component between the F814W and F160W images may indicate a spatially non-uniform dust screen preferentially reddening one portion of the system. Similar morphological differences are commonly seen in UV/optical images of ultraluminous infrared galaxies (ULIGs).

3.2. Spatially-Resolved Spectroscopy

Both Ly α and [O III] λ 5007 are spatially-extended in our two-dimensional spectra (Fig. 5). The Ly α profile shows a triangular, or delta, structure, typical of high-redshift Ly α emission: foreground neutral hydrogen from large scale outflows absorbs the blue wing of the emission line and leads to a P-Cygni profile (e.g., Dey et al. 1998). The Ly α line

of CXO52 is extended by $3''$, or $20 h_{50}^{-1}$ kpc. Extended Ly α emission is commonly seen in radio galaxies and radio-loud Type-I quasars, though not as commonly in radio-quiet Type-I quasars.

The [O III] $\lambda 5007$ emission line of CXO52 has a tadpole morphology, comprised of a head at a redshift corresponding to the other emission lines of this source, and a tail extending by $\approx 0''.5$ ($3 h_{50}^{-1}$ kpc) and $\approx 500 \text{ km s}^{-1}$. The position angle for these infrared spectra roughly align with the extended morphology seen in the *HST* images. We may be seeing rotation from CXO52, or the apparent kinematics may be due to infall/outflow. Assuming the system is in dynamic equilibrium, the mass implied by this apparent rotation is $\approx 2 \times 10^{10} M_{\odot}$.

3.3. CXO52 Compared to Other *Chandra*-Selected Type II Quasars

In both of the mega-second *Chandra* deep survey fields, at least one example of a $z > 2$ Type II quasar has been identified: Dawson et al. (2001) identify CXO HDFN J123635.6+621424 at $z = 2.011$ in the *Hubble* Deep Field North (HDF-N) and Norman et al. (2001) identify CDF-S 202 at $z = 3.700$ in the *Chandra* Deep Field South (CDF-S). Many of the properties of CXO52 are similar to these two sources: optical spectra of all three show narrow, high-ionization lines and all three show flat X-ray spectra, indicative of absorption. For CDF-S 202, Norman et al. (2001) infer a local hydrogen column with $N_H \sim 10^{24} - 10^{25} \text{ cm}^{-2}$ at the quasar redshift, based on the X-ray spectrum. The implied rest-frame, hard-band X-ray luminosity is then $L_{2-10} \sim 10^{45 \pm 0.5} \text{ ergs s}^{-1}$, slightly more luminous than CXO52. Both hard X-ray luminosities are comparable to those observed by *ASCA* for optically-selected Type I quasars (e.g., George et al. 2000). The optical/near-infrared identification of the Type II quasar in the HDF-N has a very red color, $I - K = 4.14$, similar to that of CXO52 ($I - K_s = 4.21$). Curiously, however, CDF-S 202 is quite blue with $I - K = 1.66$, perhaps due to C IV $\lambda 1549$ and He II $\lambda 1640$ contributions to the observed I -band flux.

Neither CXO52 nor CDF-S 202 are detected at radio wavelengths, while CXO HDFN J123635.6+621424 is detected in the ultradeep 1.4 GHz VLA survey of the HDF-N at a flux density of $f_{1.4\text{GHz}} = 87.7 \mu\text{Jy}$ (Richards 2000). For a typical observed radio galaxy spectral index $\alpha = -1$, where $f_{\nu} \propto \nu^{\alpha}$, the implied rest-frame 1.4 GHz radio luminosity density of CXO HDFN J123635.6+621424 is $L_{1.4\text{GHz}} = 2.5 \times 10^{31} h_{50}^{-2} \text{ ergs s}^{-1} \text{ Hz}^{-1}$, while $L_{1.4\text{GHz}} < 1.1 \times 10^{32} h_{50}^{-2} \text{ ergs s}^{-1} \text{ Hz}^{-1}$ for CDF-S 202 and $L_{1.4\text{GHz}} < 1.2 \times 10^{32} h_{50}^{-2} \text{ ergs s}^{-1} \text{ Hz}^{-1}$ for CXO52. For $\alpha = -0.5$, a typical radio spectral index for radio-loud quasars, these luminosity densities drop by a factor of ≈ 3 . Adopting the Gregg et al. (1996) cutoff value of $L_{1.4\text{GHz}} = 10^{32.5} h_{50}^{-2} \text{ ergs s}^{-1} \text{ Hz}^{-1}$ to separate radio-loud sources from radio-quiet sources, all three of these high-redshift *Chandra*-identified Type II quasars are radio-quiet. We note that more recent work from the FIRST

Bright Quasar Survey (FBQS; White et al. 2000) suggests that no strong bimodality exists between radio-loud and radio-quiet Type-I quasars.

There is one other likely Type II quasar in the deep *Chandra* fields: the mJy radio source VLA J123642+621331 has recently been detected in the soft X-ray band by *Chandra* (Brandt et al. 2001). VLA J123642+621331, which lies just outside the HDF-N, is a $f_{1.4\text{GHz}} = 470\mu\text{Jy}$ radio source (Richards 2000), shown by Waddington et al. (1999) to reside at a likely redshift $z = 4.424$. The optical spectrum is similar to a faint radio galaxy or Type II AGN ($\text{FWHM}_{\text{Ly}\alpha} = 420 \pm 75 \text{ km s}^{-1}$). The derived *unabsorbed* rest-frame X-ray luminosity of $L_{0.5-2} = 2.5 \times 10^{42} h_{50}^{-2} \text{ ergs s}^{-1}$ is below the knee of the Miyaji, Hasinger, & M.Schmidt (2000) soft X-ray luminosity function while the rest-frame 1.4 GHz specific luminosity, $L_{1.4\text{GHz}} = 7.1 \times 10^{32} h_{50}^{-2} \text{ ergs s}^{-1} \text{ Hz}^{-1}$, is classified as radio-loud according to the Gregg et al. (1996) definition. The likelihood of finding such a radio-luminous, distant galaxy within the small area of a single *Chandra* pointing is small (see §3.6).

3.4. CXO52 Compared to High-Redshift Radio Galaxies

With high-ionization emission lines with widths $\gtrsim 1000 \text{ km s}^{-1}$ and a spatially-resolved morphology, CXO52 has very similar properties to high-redshift radio galaxies (HzRGs; e.g., McCarthy 1993), the only flavor of obscured (i.e., Type-II) AGN which has been extensively studied beyond a redshift of unity. As opposed to quasars which have broad permitted lines and optical morphologies dominated by an unresolved nucleus, HzRGs have narrow ($\text{FWHM} < 2000 \text{ km s}^{-1}$) permitted lines and host galaxies which are spatially extended. Equivalent widths of forbidden lines are larger in HzRGs than in quasars.

He II $\lambda 1640$ is strongly detected in CXO52 with C IV $\lambda 1549/\text{He II } \lambda 1640 \approx 2$. This is typical of HzRGs and atypical of Type I quasars: composite HzRGs spectra show C IV $\lambda 1549/\text{He II } \lambda 1640 \simeq 1.5$ (McCarthy 1993; Stern et al. 1999), while composite quasar spectra show C IV $\lambda 1549/\text{He II } \lambda 1640 \approx 10 - 50$ (Boyle 1990; Vanden Berk et al. 2001). Assuming an $[\text{O II}] \lambda 3727/[\text{O III}] \lambda 5007$ ratio similar to HzRGs, the $[\text{O II}] \lambda 3727$ emission line luminosity of CXO52 is $\approx 5 \times 10^{42} \text{ ergs s}^{-1}$, typical of bright 3CR HzRGs (McCarthy 1993; Willott et al. 1999). We reiterate that CXO52 remains *undetected* in our radio images which, at 4.8 GHz, probe *four* orders of magnitude deeper than classical HzRG surveys such as the MIT-Greenbank survey (Bennett et al. 1986; Lawrence et al. 1986) and an order of magnitude deeper than more modern HzRG surveys such as the Leiden Berkeley Deep Survey (LBDS; Waddington et al. 2001). In many ways, CXO52 appears to be an example of an oxymoronic *radio-quiet radio galaxy*. Alternatively, just as we know of radio-loud and radio-quiet (Type-I) quasars, HzRGs simply represent the radio-loud portion of the Type-II

quasar population while CXO52 represents a rare example of a radio-quiet Type-II quasar. As discussed in §3.5, these radio-quiet Type-II quasars conceivably outnumber the HzRG population by a factor of a few: the rarity of known examples of the population, such as CXO52, may merely represent observational bias, not an inherent scarcity of the population.

The N V $\lambda 1240$ emission in CXO52 is weak, with $N V \lambda 1240 / C IV \lambda 1549 = 0.17$, approximately half what is seen in composite HzRG spectra (McCarthy 1993; Stern et al. 1999). Vernet et al. (2001) calculate photoionization models of HzRGs for a range of metallicity. The location of CXO52 in the N V/He II versus N V/C IV line diagnostic diagram (Fig. 9 of Vernet et al. 2001) implies a metallicity of $\approx 0.8Z_{\odot}$.

McCarthy, Elston, & Eisenhardt (1992), Eales & Rawlings (1993, 1996), and Evans (1998) have successfully obtained infrared spectra of HzRGs from 4 m-class telescopes and show that the line ratios are most consistent with Seyfert 2s, i.e., obscured AGN. Larkin et al. (2000) reports on NIRSPEC spectroscopy of the $z = 2.630$ HzRG MRC 2025–218. From Ly α to [O III] $\lambda 5007$, the spectrum of MRC 2025–218 is very similar to that of CXO52: both sources show narrow, high-ionization emission and have [O III] $\lambda 5007 / H\beta$ line ratios > 10 , consistent with a Seyfert 2 galaxy. However, a K -band spectrum of MRC 2025–218 reveals broad (FWHM = 9300 km s^{-1}) H α emission, implying this HzRG is more like a high-luminosity analog of a Seyfert 1.8 than the high-luminosity analog of a Seyfert 2. It is conceivable a longer-wavelength spectrum of CXO52 would reveal broad H α at $2.8\mu\text{m}$, but such an observation is beyond current capabilities. On the other hand, Motohara et al. (2001) report on near-infrared spectra of the $z = 2.39$ HzRG LBDS 53W002, obtained with Subaru telescope. They detect the rest-frame optical emission lines from [O II] $\lambda 3727$ to H α , finding a Seyfert 2-like [O III] $\lambda 5007 / H\beta$ line ratio, and they do not resolve H α (FWHM $\lesssim 700 \text{ km s}^{-1}$).

As initially pointed out by Lilly & Longair (1982), there exists a surprisingly tight correlation between the $2.2 \mu\text{m}$ (K band) infrared magnitude and galaxy redshift for HzRGs, despite significant morphological evolution (van Breugel et al. 1998) and dramatic k -correction effects out to $z = 5.19$, the highest redshift for which a HzRG has been identified (van Breugel et al. 1999). At $z = 5.19$, K samples the rest-frame U -band. With $K = 20.5$, CXO52 is significantly fainter at $2 \mu\text{m}$ than the typical HzRG which has $K \approx 19$ at $z \approx 3$ (e.g., De Breuck et al. 2001). Does this teach us something about the host galaxies of radio-quiet versus radio-loud Type-II quasars? Though the conventional wisdom that radio-loud Type-I quasars live in ellipticals and radio-quiet Type-I quasars live in spirals has been debunked (McLeod & McLeod 2001, and references therein), the following correlations appear to remain true: (1) the fraction of Type-I quasars inhabiting elliptical host galaxies increases with nuclear luminosity, and (2) radio-loud Type-I quasars have brighter host galaxies than radio-quiet

Type-I quasars (e.g., Boyce et al. 1998). Unified models of AGN remain uncertain as to the cause of these correlations. One suggestion is that dust in late-type systems quenches radio jets, preventing their escape into the intergalactic medium. In another model, Wilson & Colbert (1995) suggest radio-loud AGN are the products of coalescing supermassive black holes in galaxy mergers, a process which would result in rapidly spinning black holes capable of generating highly collimated jets and powerful radio sources. Such models would naturally explain the difference in host morphology for radio-loud and radio-quiet Type-I quasars. The relative K -band faintness of CXO52 compared to HzRGs at similar redshift may simply indicate that obscured AGN obey the same correlations.

3.5. Search Techniques for Type II Quasars

Because they are much less luminous than Type I quasars at optical wavelengths, Type II quasars suffer from a dearth of observational study. In the low-redshift Universe, large sky surveys have begun to identify these sources due to their unusual colors caused by high-equivalent width emission features (e.g., Djorgovski et al. 2001a). The radio-loud portion of the high-redshift Type II quasar population has been identified through dedicated, often heroic (e.g., Spinrad 1972 – 1998), follow-up of radio surveys. However, only $\sim 10 - 15\%$ of Type I quasars are radio-loud, with no evidence of redshift dependence out to $z \gtrsim 4$ (Stern et al. 2000b). Are HzRGs just the tip of the obscured, Type II quasar iceberg? Is there a population of radio-quiet Type II quasars remaining to be studied with more than six times the space density of HzRGs? How else might obscured quasars be identified, and what can we say about the density of high-redshift Type II quasars from the current samples?

As seen from the examples of CXO52 and the Type II quasars in the *Chandra* mega-second fields, obscured quasars are readily identified from deep X-ray surveys. Deep, multi-band imaging surveys are also sensitive to high-redshift, Type-II quasars: though they are significantly fainter than unobscured quasars, Type-II quasars are readily identified in surveys for distant galaxies. Indeed, as mentioned in §2.1, CXO52 was initially identified in this manner, prior to *Chandra* imaging of the Lynx field. We have found a similar source at $z = 2.82$ in the Pisces field of the SPICES survey (Bower et. al., in preparation).

Due to their high equivalent width, narrow features, obscured quasars can also be identified in narrow-band imaging surveys. Several such surveys are currently in progress with the goal of identifying high-redshift Ly α emission due to its high equivalent width (e.g., Rhoads et al. 2001; Hu, McMahon, & Cowie 1999). Magnitude-limited surveys rarely find galaxies with emission lines whose rest-frame equivalent width is larger than ≈ 100 Å, the exceptions being Ly α and H α which can have rest-frame equivalent widths of 200 Å and 2000 Å, re-

spectively, in a young, star-forming galaxy (e.g., Charlot & Fall 1993). $\text{H}\alpha$ is easily identified from the neighboring emission lines of $[\text{N II}] \lambda 6584$ and $[\text{S II}] \lambda\lambda 6716, 6731$ (but see Stockton & Ridgway 1998), as well as the broad-band SED of the galaxy. With the $(1+z)$ boosting of observed equivalent width due to redshifting, galaxies identified with $W_\lambda \gtrsim 200 \text{ \AA}$ should almost exclusively be identified with high-redshift $\text{Ly}\alpha$ (but see Stern et al. 2000a). However, comparing emission-line-selected samples to magnitude-limited samples is not quite fair: it is quite conceivable that new populations will appear from these emission-line surveys. In particular, the known Type II quasars all show high equivalent width emission (e.g., Fig. 3). Obscured AGN, interesting in their own right, are apt to contaminate these high-redshift $\text{Ly}\alpha$ surveys. Indeed, Rhoads et al. (2001), in their Large-Area Lyman-Alpha (LALA) survey, report an object with narrow $\text{C IV} \lambda 1549$, $\text{He II} \lambda 1640$, and $[\text{O III}] \lambda 1663$ emission at $z = 2.57$, likely classifiable as a Type II AGN.

3.6. The Density of Type II Quasars and their Contribution to the XRB

Moran et al. (2001) recently derived the local X-ray volume emissivity of Seyfert 2 galaxies and show that under reasonable assumptions regarding the spectral energy distribution and evolutionary history of obscured AGN, they provide an excellent match to the spectrum and intensity of the cosmic X-ray background (XRB). Before the XRB problem can be considered solved, however, these assumptions must be tested. We next consider whether the observed numbers of high-redshift Type II quasars identified in the deepest *Chandra* fields are consistent with expectations and predictions.

As one estimate of the expected surface density of Type II quasars, we can begin with the known distribution of radio-loud AGN. Willott et al. (2001) have recently provided the most accurate determination of the radio luminosity function (RLF) to date, derived from several low-frequency surveys. They fit the RLF with a dual-population model comprised of: (1) low-luminosity radio sources, typically showing weak emission lines; and (2) high-luminosity radio sources, associated with HzRGs and quasars. It is this latter population that is of interest here. For $2 < z < 5$, Model C of Willott et al. (2001) reports a surface density of 1.16×10^{-3} high-luminosity radio sources per arcminute², corresponding to 0.33 such sources per $17' \times 17'$ *Chandra*/ACIS-I field. Approximately 40% of the high-luminosity radio sources are broad-lined quasars (Willott et al. 2000), implying 0.20 narrow-lined HzRGs per *Chandra* field. Stern et al. (2000b) show that $\approx 12\%$ of optically-selected broad-lined quasars are radio-loud, with little redshift dependence in this fraction out to $z \gtrsim 4$. If Type II quasars have the same radio-loud fraction, we would expect *one to two* Type II quasars per *Chandra* field at $2 < z < 5$. Indeed, this is exactly what has been found from preliminary

investigations of the three best-studied, deep *Chandra* fields!

We can also estimate the expected surface density of high-redshift Type II quasars by scaling from better-constrained Type I quasar luminosity functions (QLFs). Using the same assumptions about radio-loudness fraction as before, the Willott et al. (2001) high-luminosity radio luminosity function predicts 1.1 unobscured quasars at $2 < z < 5$ per *Chandra* field. The Miyaji et al. (2000) Type I soft X-ray luminosity function predicts 1.8 unobscured, luminous ($L_{0.5-2} \geq 10^{44.5} \text{ ergs s}^{-1}$) quasars at $2 < z < 5$ per *Chandra* field, similar to the radio prediction. The Sloan Digital Sky Survey (SDSS) high-redshift, luminous optical QLF (Fan et al. 2000) predicts slightly more unobscured quasars per *Chandra* field: it predicts 1.86 such sources with absolute magnitude at 1450 Å, $M_{1450} < -24$ and 7.92 such sources with $M_{1450} < -23$. These numbers should be considered estimates, however, as the SDSS QLF has been derived using a sample of quasars at higher redshift ($3.6 < z < 5.0$) and brighter absolute magnitude ($-27.5 < M_{1450} < -25.5$). We combine the above results to predict approximately one or two $2 < z < 5$ Type I quasars per *Chandra* field. As a baseline we assume a ratio of obscured (Type II) to unobscured (Type I) high-redshift quasars of 3:2, matching the Willott et al. (2000) high-luminosity radio results, implying one to three $2 < z < 5$ Type II quasars per *Chandra* field. If X-ray follow-up of the deep *Chandra* fields finds a substantially larger surface density of high-redshift Type II quasars, this would imply that the ratio of obscured to unobscured luminous AGN at high-redshift was different, with some dependency on the radio properties of the source. The implications would be significant for studies of the XRB and AGN unification scenarios.

4. Conclusions

We report the discovery of CXO52, an obscured, or Type II quasar at $z = 3.288$, identified independently both as a *B*-band Lyman-dropout galaxy and as a hard X-ray source in a 185 ks *Chandra* exposure. Besides (1) X-ray selection and (2) color-selection, high-redshift Type II quasars are also identifiable from (3) radio surveys and (4) narrow-band imaging surveys. This population of misdirected or obscured quasars, long thought necessary to explain the X-ray background and demanded by unified models of AGN, are finally being identified in both their radio-quiet and radio-loud flavors. They are likely more populous than the well-studied unobscured, Type I quasar population. *Chandra* has now identified examples of radio-quiet, high-redshift, Type II quasars in each of deepest fields. Preliminary results are consistent with the simple assumption that the ratio of Type II systems to Type I systems is the same for both radio-loud and radio-quiet systems at high redshift, namely a ratio of 3:2.

We report on the panchromatic properties of CXO52, finding the broad-band SED is similar to that of local composite Seyfert 2 galaxies. Morphologically, CXO52 is resolved and somewhat elongated, distinctly different in appearance from traditional Type I quasars. Optical and near-infrared spectra of CXO52 obtained with the Keck telescopes show strong, narrow emission lines with ratios similar to HzRGs and Seyfert 2s.

Type II AGN are luminous in the mid-infrared: radiation which is absorbed by gas and dust in the rest-frame ultraviolet/optical escapes as thermal emission in the mid-infrared. Several examples of obscured, reddened quasars have been identified from shallow, wide-area surveys such as FIRST and 2MASS (e.g., Becker et al. 1997; Gregg et al. 2001). The *Space Infrared Telescope Facility (SIRTF)* will identify the unlensed, less extreme portions of this population. To first order, luminous AGN are isotropic at radio, mid- to far-infrared, and hard X-ray wavelengths, though their ultraviolet/optical properties depend heavily upon orientation. Though it is extremely faint optically with $R = 25$, CXO52 should be luminous in the mid-infrared with $S_{3.6\mu\text{m}} \approx 50\mu\text{Jy}$ and $S_{24\mu\text{m}} \approx 1.5 \text{ mJy}$, determined from the scaled Schmitt et al. (1997) Seyfert 2 SED (Fig. 2). These flux levels are easily detectable in a shallow *SIRTF* observation. Surveys with *SIRTF* and the new generation of X-ray satellites should help provide an unbiased census of AGN in the Universe, thereby testing models of the XRB and providing a history of accretion-driven energy production in the Universe.

We gratefully acknowledge Carlos De Breuck for carefully reading the manuscript and providing insightful comments. We also thank Aaron Barth for helpful suggestions. The authors wish to extend special thanks to those of Hawaiian ancestry on whose sacred mountain we are privileged to be guests. Without their generous hospitality, many of the observations presented herein would not have been possible. We thank Andrea Gilbert for assisting with the NIRSPEC spectroscopy. Some of the LRIS data were obtained in the course of a collaborative project with S.G. Djorgovski. We thank Niruj Mohan for providing the 4.8 GHz VLA image. Support for this work was provided by the National Aeronautics and Space Administration through *Chandra* Award Number GO0-1082B issued by the *Chandra* X-Ray Observatory Center, which is operated by the Smithsonian Astrophysical Observatory for and on behalf of NASA under contract NAS8-39073. The work of DS and PE were carried out at the Jet Propulsion Laboratory, California Institute of Technology, under a contract with NASA. The work of SD was performed under the auspices of the U.S. Department of Energy, National Nuclear Security Administration by the University of California, Lawrence Livermore National Laboratory under contract No. W-7405-Eng-48. E.C.M. is supported by NAS through *Chandra* Fellowship grant PF8-10004, awarded by the *Chandra* X-Ray Center, which is operated by the Smithsonian Astrophysical Observatory for NASA under contract NAS 8-39073. This work has also been supported by the following grants: NSF

grant AST00-71048 (MD), IGPP-LLNL UCRP grant #02-AP-015 (SD), NSF CAREER grant AST 9875448 (RE), NASA grant NAG 5-6035 (DJH), and NSF grant AST 95–28536 (HS).

REFERENCES

Almaini, O., Boyle, B. J., Griffiths, R. E., Shanks, T., Stewart, G. C., & Georgantopoulos, I. 1995, MNRAS, 277, L31

Antonucci, R. 1993, ARA&A, 31, 473

Arnaud, K. A. 1996, in *Astronomical Data Analysis Software and Systems V*, ed. J. G. Jacoby & J. Barnes, Vol. 101 (San Francisco: ASP Conference Series), 17

Becker, R. H., Gregg, M. D., Hook, I. M., McMahon, R. G., White, R. L., & Helfand, D. J. 1997, ApJ, 479, 93

Becker, R. H., White, R. L., & Helfand, D. J. 1995, ApJ, 450, 559

Becker, R. H. et al. 2001, AJ, submitted, astro-ph/0108097

Bennett, C. L., Lawrence, C. R., Burke, B. F., Hewitt, J. N., & Mahoney, J. 1986, ApJS, 61, 1

Boroson, T. A. & Green, R. F. 1992, ApJS, 80, 109

Boyce, P. J., Disney, M. J., Blades, J. C., Boksenberg, A., Crane, P., Deharveng, J. M., Macchetto, F. D., Mackay, C. D., et al., 1998, MNRAS, 298, 121

Boyle, B. J. 1990, MNRAS, 243, 231

Boyle, B. J., Almaini, O., Georgantopoulos, I., Blair, A. J., Stewart, G. C., Griffiths, R. E., Shanks, T., & Gunn, K. F. 1998, MNRAS, 297, L53

Brandt, W. N. et al. 2001, AJ, 122, 1

Charlot, S. & Fall, S. M. 1993, ApJ, 378, 471

Comastri, A., Setti, G., Zamorani, G., & Hasinger, G. 1995, A&A, 296, 1

Dawson, S., Stern, D., Bunker, A. J., Spinrad, H., & Dey, A. 2001, AJ, accepted [astro-ph/0105043]

De Breuck, C., van Breugel, W., Stanford, S. A., Röttgering, H., Miley, G., & Stern, D. 2001, AJ, submitted

Dey, A., Graham, J. R., Ivison, R. J., Smail, I., Wright, G. S., & Liu, M. C. 1999, ApJ, 519, 610

Dey, A., Spinrad, H., Stern, D., Graham, J. R., & Chaffee, F. 1998, ApJ, 498, L93

Djorgovski, S. G., Castro, S. M., Stern, D., & Mahabal, A. A. 2001a, ApJ, submitted, astro-ph/0108069

Djorgovski, S. G., Gal, R. R., Odewahn, S. C., de Calvalho, R. R., Brunner, R., Longo, G., & Scaramella, R. 1999, in *Wide Field Surveys in Cosmology*, ed. Y. Mellier & S. Colombi (Gif sur Yvette: Editions Frontières), 89

Djorgovski, S. G., Mahabal, A. A., Brunner, R. J., Gal, R. R., Castro, S., de Calvalho, R. R., & Odewahn, S. C. 2001b, in *Virtual Observatories of the Future*, ed. R. J. Brunner, S. G. Djorgovski, & A. Szalay, Vol. 225 (San Francisco: ASP Conference Series), 52

Eales, S. & Rawlings, S. 1993, ApJ, 411, 67

—. 1996, ApJ, 460, 68

Eisenhardt, P., Elston, R., Stanford, S. A., Stern, D., Wu, K. L., Connolly, A., & Spinrad, H. 2001, AJ, in preparation

Elizalde, F. & Steiner, J. E. 1994, MNRAS, 268, L47

Evans, A. S. 1998, ApJ, 498, 553

Fan, X. et al. 1999, AJ, 118, 1

—. 2000, AJ, 120, 1167

—. 2001, AJ, submitted [astro-ph/0108063]

Fowler, A. M., Gatley, I., Stuart, F., Joyce, R. R., & Probst, R. G. 1988, SPIE, 972, 107

Georgantopoulos, I., Almaini, O., Shanks, T., Stewart, G. C., Griffiths, R. E., Boyle, B. J., & Gunn, K. F. 1999, MNRAS, 305, 125

George, I. M., Turner, T. J., Yaqoob, T., Netzer, H., Laor, A., Mushotzky, R. F., Nandra, K., & Takahashi, T. 2000, ApJ, 531, 52

Goodrich, R. W. 1989, ApJ, 342, 234

Gregg, M. D., Becker, R. H., White, R. L., Helfand, D. J., McMahon, R. G., & Hook, I. M. 1996, AJ, 112, 407

Gregg, M. D., Lacy, M., White, R. L., Glikman, E., Helfand, D. J., Becker, R. H., & Brotherton, M. S. 2001, ApJ, in press [astro-ph/0107441]

Halpern, J. P., Eracleous, M., & Forster, K. 1998, ApJ, 501, 103

Halpern, J. P. & Moran, E. C. 1998, ApJ, 494, 194

Halpern, J. P., Turner, T. J., & George, I. M. 1999, MNRAS, 307, L47

Ho, L. C. 1999, Adv. in Space Research, 23, 813

Ho, L. C. & Ulvestad, J. S. 2001, ApJS, 133, 77

Holden, B., Stanford, S. A., Rosati, P., Tozzi, P., Eisenhardt, P. R. M., & Spinrad, H. 2001, AJ, in press (August)

Hu, E. M., McMahon, R. G., & Cowie, L. L. 1999, ApJ, 522, 9

Kells, W., Dressler, A., Sivaramakrishnan, A., Carr, D., Koch, E., Epps, H., Hilyard, D., & Pardeilhan, G. 1998, PASP, 110, 1487

Kennefick, J. D., Djorgovski, S. G., & de Calvalho, R. R. 1995, AJ, 110, 2553

Kriss, G. 1994, in *Astronomical Data Analysis Software and Systems III*, Vol. 61 (San Francisco: ASP Conference Series), 437

Larkin, J. E. et al. 2000, ApJ, 533, L61

Lawrence, C. R., Readhead, A. C. S., Moffet, A. T., & Birkinshaw, M. 1986, ApJS, 61, 105

Lilly, S. J. & Longair, M. S. 1982, MNRAS, 199, 1053

Madau, P., Ghisellini, G., & Fabian, A. C. 1994, MNRAS, 270, 17

Massey, P. & Gronwall, C. 1990, ApJ, 358, 344

McCarthy, P. J. 1993, ARA&A, 31, 639

McCarthy, P. J., Elston, R., & Eisenhardt, P. 1992, ApJ, 387, L29

McCarthy, P. J., Spinrad, H., & van Breugel, W. 1995, ApJS, 99, 27

McLean, I. S. et al. 1998, SPIE, 3354, 566

McLeod, K. K. & McLeod, B. A. 2001, ApJ, 546, 782

Meurs, E. J. A. 1982, *The Seyfert galaxy population — A radio survey; luminosity functions, related objects* (Univ. Leiden: Ph.D. thesis)

Meurs, E. J. A. & Wilson, A. S. 1984, A&A, 136, 206

Miyaji, T., Hasinger, G., & M.Schmidt. 2000, A&A, 353, 25

Moran, E. C., Kay, L. E., Davis, M., Filippenko, A. V., & Barth, A. J. 2001, ApJ, in press, astro-ph/0106519

Motohara, K. et al. 2001, PASJ, in press, astro-ph/0104473

Nandra, K. & Pounds, K. A. 1994, MNRAS, 268, 405

Norman, C. et al. 2001, ApJ, submitted, astro-ph/0103198

Oke, J. B., Cohen, J. G., Carr, M., Cromer, J., Dingizian, A., Harris, F. H., Labrecque, S., Lucinio, R., et al., 1995, PASP, 107, 375

Osterbrock, D. E. & Pogge, R. W. 1985, ApJ, 297, 166

Osterbrock, D. E. & Shaw, R. A. 1988, ApJ, 327, 89

Rhoads, J. E., Malhotra, S., Dey, A., Stern, D., Spinrad, H., & Jannuzi, B. T. 2001, ApJ, 545, L85

Richards, E. A. 2000, ApJ, 533, 611

Riess, A. G. et al. 2001, ApJ, in press; astro-ph/0104455

Rosati, P., della Ceca, R., Norman, C., & Giacconi, R. 1998, ApJ, 492, L21

Rosati, P., Stanford, S. A., Eisenhardt, P. R., Elston, R., Spinrad, H., Stern, D., & Dey, A. 1999, AJ, 118, 76

Schmitt, H. R., Kinney, A. L., Calzetti, D., & Storchi-Bergmann, T. 1997, AJ, 114, 592

Spinrad, H., Stern, D., Bunker, A. J., Dey, A., Lanzetta, K., Yahil, A., Pascarelle, S., & Fernández-Soto, A. 1998, AJ, 116, 2617

Stanford, S. A., Elston, R., Eisenhardt, P. R. M., Spinrad, H., Stern, D., & Dey, A. 1997, AJ, 114, 2232

Stanford, S. A., Rosati, P., Holden, B., Tozzi, P., Eisenhardt, P. R. M., & Spinrad, H. 2001, *ApJ*, 552, 504

Steidel, C. S., Giavalisco, M., Dickinson, M., & Adelberger, K. L. 1996, *AJ*, 112, 352

Stern, D., Bunker, A. J., Spinrad, H., & Dey, A. 2000a, *ApJ*, 537, 73

Stern, D., Connolly, A., Eisenhardt, P., Elston, R., Holden, B., Rosati, P., Stanford, S. A., Spinrad, H., et al., 2001a, in *Deep Fields 2000* (Berlin: Springer Verlag), in press [astro-ph/0012146]

Stern, D., Dey, A., Spinrad, H., Maxfield, L. M., Dickinson, M. E., Schlegel, D., & González, R. A. 1999, *AJ*, 117, 1122

Stern, D., Djorgovski, S. G., Perley, R., de Carvalho, R., & Wall, J. 2000b, *AJ*, 132, 1526

Stern, D. & Spinrad, H. 1999, *PASP*, 111, 1475

Stern, D., Spinrad, H., Eisenhardt, P., Bunker, A. J., Dawson, S., Stanford, S. A., & Elston, R. 2000c, *ApJ*, 533, L75

Stern, D., Tozzi, P., Stanford, S. A., Rosati, P., Holden, B., Eisenhardt, P., Elston, R., Wu, K. L., et al., 2001b, *AJ*, submitted

Stocke, J., Liebert, J., Maccacaro, T., Griffiths, R. E., & Steiner, J. E. 1982, *ApJ*, 252, 69

Stockton, A. & Ridgway, S. E. 1998, *AJ*, 115, 1340

Thompson, R., Storrie-Lombardi, L. J., Weymann, R. J., Rieke, M. J., Schneider, G., Stobie, E., & Lytle, D. 1999, *AJ*, 117, 17

Trauger, S. et al. 1994, *ApJ*, 435, 3

Urry, C. M. & Padovani, P. 1995, *PASP*, 107, 803

van Breugel, W., De Breuck, C., Stanford, S. A., Stern, D., Röttgering, H., & Miley, G. 1999, *ApJ*, 518, L61

van Breugel, W., Stanford, S. A., Spinrad, H., Stern, D., & Graham, J. R. 1998, *ApJ*, 502, 614

van Dokkum, P. G., Stanford, S. A., Holden, B. P., Eisenhardt, P. R., Dickinson, M., & Elston, R. 2001, *ApJ*, in press

Vanden Berk, D. E. et al. 2001, *AJ*, in press, astro-ph/0105231

Vernet, J., Fosbury, R. A. E., Villar-Martin, M., Cohen, M. H., Cimatti, A., di Serego Alighieri, S., & Goodrich, R. W. 2001, A&A, 366, 7

Waddington, I., Dunlop, J. S., Peacock, J. A., & Windhorst, R. A. 2001, MNRAS, submitted; astro-ph/0107048

Waddington, I., Windhorst, R. A., Cohen, S. H., Partridge, R. B., Spinrad, H., & Stern, D. 1999, ApJ, 526, 77

Weisskopf, M. C., O'dell, S. L., & van Speybroeck, L. P. 1996, SPIE, 2805, 2

White, R. L. et al. 2000, ApJS, 126, 133

Willott, C. J., Rawlings, S., Blundell, K. M., & Lacy, M. 1999, MNRAS, 309, 1017

—. 2000, MNRAS, 316, 449

Willott, C. J., Rawlings, S., Blundell, K. M., Lacy, M., & Eales, S. A. 2001, MNRAS, 322, 536

Wilson, A. S. & Colbert, E. J. M. 1995, ApJ, 438, 62

Table 1. Photometry of CXO52

Observed Bandpass	Restframe Bandpass	Observed Magnitude	Flux Density (μ Jy)	Detector/ Instrument
2–10 keV	25.7 keV	...	$(1.806 \pm 0.444) \times 10^{-4}$	<i>Chandra</i> /ACIS
0.5–2 keV	5.4 keV	...	$(1.882 \pm 0.405) \times 10^{-4}$	<i>Chandra</i> /ACIS
<i>B</i>	1010 Å	$27.18_{-0.31}^{+0.43}$	0.053 ± 0.018	KPNO/PFC
<i>R</i>	1510 Å	$24.95_{-0.20}^{+0.24}$	0.313 ± 0.062	KPNO/PFC
F814W [†]	1900 Å	$24.81_{-0.22}^{+0.18}$	0.433 ± 0.082	<i>HST</i> /WFPC2
<i>I</i>	1915 Å	$24.69_{-0.31}^{+0.44}$	0.318 ± 0.106	KPNO/PFC
z_{AB}^{\dagger}	2190 Å	$24.83_{-0.31}^{+0.43}$	0.425 ± 0.140	KPNO/PFC
<i>J</i>	2660 Å	> 22.79	< 1.212	KPNO/IRIM
F160W [†]	3730 Å	23.78 ± 0.30	1.117 ± 0.313	<i>HST</i> /NICMOS
<i>K_s</i>	5040 Å	$20.48_{-0.16}^{+0.19}$	4.066 ± 0.650	KPNO/IRIM
$3.6 \mu\text{m}^{\ddagger}$	8400 Å	...	45	<i>SIRTF</i> /IRAC
$4.5 \mu\text{m}^{\ddagger}$	$1.1 \mu\text{m}$...	70	<i>SIRTF</i> /IRAC
$5.8 \mu\text{m}^{\ddagger}$	$1.4 \mu\text{m}$...	130	<i>SIRTF</i> /IRAC
$8.0 \mu\text{m}^{\ddagger}$	$1.9 \mu\text{m}$...	270	<i>SIRTF</i> /IRAC
$24 \mu\text{m}^{\ddagger}$	$5.6 \mu\text{m}$...	1500	<i>SIRTF</i> /MIPS
4.8 GHz	20.6 GHz	...	< 40	VLA
1.4 GHz	6.0 GHz	...	< 1000	VLA

[†]Observed magnitude in the AB system.

[‡]Predicted, assuming local Schmitt et al. (1997) Seyfert 2 SED.

Note. — Optical/near-infrared photometry is determined for 3" diameter apertures. Unless otherwise noted, optical/near-infrared magnitudes are in the Vega system. CXO52 remains undetected in our *J*-band image; we list the 3σ limit for the same aperture instead.

Table 2. Emission-Line Measurements of CXO52

Line	λ_{obs} (Å)	Redshift	Flux (10^{-17} ergs cm $^{-2}$ s $^{-1}$)	FWHM (km s $^{-1}$)	$W_{\lambda,\text{rest}}$ (Å)
O VI $\lambda 1035$	4450:	3.300:	1.5:	2640:	120:
Ly α	5217.3 ± 0.3	3.291	18.9 ± 0.4	1520 ± 30	2100 ± 40
N V $\lambda 1240$	5311:	3.283:	0.6:	1820:	50:
Si IV/O IV] $\lambda 1403$	6009:	3.283:	0.4:	1320:	30:
C IV $\lambda 1549$	6639.2 ± 0.9	3.285	3.5 ± 0.2	1350 ± 90	350 ± 20
He II $\lambda 1640$	7030.4 ± 1.5	3.287	1.7 ± 0.2	940 ± 140	170 ± 20
O III] $\lambda 1663$	7130.0 ± 4.2	3.287	0.9 ± 0.3	1290 ± 330	90 ± 30
C III] $\lambda 1909$	8170.5 ± 1.4	3.280	2.1 ± 0.2	1090 ± 140	420 ± 40
H β	20847.2 ± 4.2	3.289	1.2 ± 0.8	170 ± 130	20 ± 15
[O III] $\lambda 4959$	21269.3 ± 3.4	3.289	3.7 ± 1.2	300 ± 71	50 ± 20
[O III] $\lambda 5007$	21472.5 ± 0.7	3.288	14.4 ± 0.7	430 ± 30	380 ± 20

Note. — All measurements are based on single Gaussian fits to the emission lines assuming a flat (in f_{λ}) continuum. Line velocity widths have been deconvolved by the instrument resolution. Parameters with colons indicate uncertain measurements. Rest-frame equivalent widths $W_{\lambda,\text{rest}}$ assume $z = 3.288$.

This figure "f1a.gif" is available in "gif" format from:

<http://arxiv.org/ps/astro-ph/0111513v1>

This figure "f1b.gif" is available in "gif" format from:

<http://arxiv.org/ps/astro-ph/0111513v1>